The origin of abyssal peridotites: A reinterpretation of constraints based on primary bulk compositions

Article *in* Earth and Planetary Science Letters · August 1999

DOI: 10.1016/S0012-821X(99)00130-2

CITATIONS
90

READS
76

2 authors, including:

John Beckett
California Institute of Technology
170 PUBLICATIONS **2,264** CITATIONS

SEE PROFILE

DocuServe

Electronic Delivery Cover Sheet

Caltech Library Services

ELSEVIER

Earth and Planetary Science Letters 171 (1999) 49–61

EPSL

www.elsevier.com/locate/epsl

The origin of abyssal peridotites: a reinterpretation of constraints based on primary bulk compositions

Michael B. Baker *, John R. Beckett

Division of Geological and Planetary Sciences, California Institute of Technology, MC 170-25, 1200 E California Blvd, Pasadena, CA 91125, USA

Received 13 July 1998; revised version received 1 June 1999; accepted 2 June 1999

Abstract

We calculated primary bulk compositions for a global suite of abyssal peridotites using primary mineral modes and either analyzed or calculated phase compositions. The latter were obtained through correlations between reported mineral compositions and modal olivine contents. Both the modal data and the mineral compositions were averaged by dredge site, drill hole, or fracture zone (FZ) depending on the amount of available data. Our calculated abyssal peridotite compositions yield major-element oxide-MgO trends that are generally in good agreement with those based on compilations of ultramafic nodules and peridotite massifs. In particular, we find no statistically significant correlation between FeO^* (total Fe as FeO) and MgO and, therefore, no evidence for significant olivine accumulation. Previous reports of a positive correlation reflect an artifact of the regressions used to calculate missing phase compositions and result in a relationship between the Mg# of olivine and modal olivine abundance that is inconsistent with observed variations in abyssal peridotites. There is a slight positive correlation between bulk FeO^* and MgO if individual thin sections are used to derive the mineral composition versus modal olivine regressions, but the large grain sizes and heterogeneous distributions of phases within abyssal peridotites make it unlikely that individual thin section modes accurately reflect phase proportions in meter-sized dredge-haul samples. The variability of Na and Ti contents in pyroxenes from plagioclase-free abyssal peridotites suggests to us, as it has to other workers, that a majority of these samples interacted to varying degrees with small amounts of melt. On the other hand, lower bounds on Na and Ti contents in the pyroxenes at a given dredge site as a function of modal olivine content are broadly consistent with calculated partial melting residues. Thus, abyssal peridotites may retain information both on the original partial melting process and on concurrent or later interactions with partial melts from other sources.

Keywords: peridotites; mineral composition; partial melting; mid-ocean ridge basalts; igneous rocks; genesis

1. Introduction

Abyssal peridotites are extensively altered pieces of oceanic mantle that have been sampled from each of the major ridge systems in the ocean basins [1,2]. They range in modal composition from spinel lherzolite to dunite, and are widely interpreted as being residues complementary to mid-ocean ridge basalts (MORB) [3,4]. As residues, they provide clues to the nature of melting processes beneath mid-ocean ridges. For example, trace-element abundances in clinopyroxenes from abyssal peridotites led Johnson et al. [4] and Johnson and Dick [5] to suggest that

* Corresponding author. Fax: +1 626 568 0935; E-mail: mikeb@gps.caltech.edu

0012-821X/99/$ – see front matter
PII: S0012-821X(99)00130-2

MORBs represent aggregated liquids produced during polybaric near-fractional melting. Kelemen et al. [6] utilized mineral compositions from a variety of rocks including abyssal peridotites to support their conclusion that while the bulk of MORB partial melts move through high-permeability dunite channels, some liquids move via diffuse porous flow in the lherzolite/harzburgite regions between these channels.

Although most of the important constraints on MORB petrogenesis derived from abyssal peridotites are based on mineral chemistry [4,5], bulk compositions could, in principle, be equally valuable. The fact that they have received less attention is due to the pervasive serpentinization of nearly all abyssal peridotites. Attempts to lift this veil of alteration and determine primary bulk compositions invariably rely on mineral modes and the compositions of relict phases, an approach pioneered by Dick and co-workers [3,7]. Unfortunately, reported modes are rarely accompanied by analytical data on all of the primary phases, usually because of difficulties in finding relict crystals. Thus, for many abyssal peridotites it is necessary to infer the compositions of one or more totally altered phases in order to calculate a primary bulk composition. Niu et al. [8] addressed this problem via regressions relating the composition of clinopyroxene, the most commonly analyzed silicate, to those of other primary phases. Using modal data and phase compositions from the literature, they calculated bulk compositions for 132 thin section modes. Their most remarkable result, a strong positive correlation between bulk FeO^*, $(FeO^*)^{bulk}$, and $(MgO)^{bulk}$, led them to postulate that abyssal peridotites have experienced extensive olivine addition by upwelling melts at shallow levels within the mantle.

In this paper, we present calculated primary bulk compositions for a global suite of abyssal peridotites. We use a different approach than Niu et al. [8] for obtaining the compositions of unanalyzed phases and adopt a different philosophy concerning sample size. For the major elements, our bulk compositions are consistent with regressions based on mantle nodules and alpine peridotites. In particular, FeO^*–MgO data define a nearly horizontal trend and, thus, we see no evidence for extensive olivine accumulation in abyssal peridotites. Finally, we compare our calculated bulk compositions to residues expected from adiabatic near-fractional melting and consider the possible role of diffuse porous flow in the evolution of these mantle samples.

2. Calculating bulk compositions of abyssal peridotites

2.1. Petrography of abyssal peridotites and sample selection

The majority of abyssal peridotites are coarse-grained rocks (~0.1–1.0 cm) that are extensively altered (70–80% on average) [1] and show varying degrees of deformation and primary phase heterogeneity [1,9,10]. Based on relicts and pseudomorphs, most abyssal peridotites were originally spinel lherzolites or harzburgites. Dunites and clinopyroxene-free harzburgites are relatively rare and plagioclase, where present, is usually taken to indicate a trapped melt [7]. Since our principal interest lay in reconstructing residues of mantle partial melting, we avoided thin sections (or site averages) with >2 vol% plagioclase. This cutoff is admittedly arbitrary but we were unable to discern any systematic differences in mineral compositions among thin sections at a given locality that contained very small amounts of modal plagioclase. Serpentinization and marine weathering are potentially more serious problems for calculating the primary bulk compositions of abyssal peridotites. These alteration processes are generally not isochemical with respect to components other than water [11,12], and it is, therefore, difficult to determine relative volumes of expansion for individual phases. This effect has not been rigorously incorporated into any calculations of primary bulk compositions of abyssal peridotites [1,7,8,13–15], and in the absence of better controls on relative volumes of expansion we have, in general, also ignored it. Dick and Natland [16] provide two sets of primary modes for samples from ODP 895 (one set based on raw point counts and another corrected for alteration), and we briefly discuss the effect of their volume correction on the calculated bulk composition.

The proportions of primary phases can be quite variable in samples from a given dredge site [1,7] or in closely associated sections of drill core [10].

In ODP hole 670A for example, the variation in olivine content (69–99 vol%) is thought to reflect the large size and heterogeneous distribution of orthopyroxene–clinopyroxene clusters [10]. Such variability affects the surface area that must be point counted to yield a representative sample. Johnson and Dick [5] stated that ten large (24 cm^2) thin sections are adequate for a dredge-site average, and we obtained similar estimates by applying a 'rule-of-thumb' analysis for structureless plutonic rocks [17] and the treatment of Bayly [18] to the sketched surface of an abyssal peridotite from DSDP Hole 395 [9]. Although this analysis is at best semi-quantitative, it motivated our choice of sample size. For the data of Dick and co-workers, we used the site averages compiled in [1], calculated dredge-site averages for the data of [5], and averaged the modes from ODP Hole 895 [16]. With respect to the data of [1], we included only dredge sites for which there were three or more thin sections. This is substantially less than ten but very few of their sites have modal data for ten or more thin sections. For the data of Bonatti and co-workers [2,15], we used their reported fracture zone or DSDP drill hole averages. However, individual thin section modes were reported for the Western Romanche Fracture Zone [19], and here we averaged the modes of the group 1 samples. Our final data set consists of modes from 36 dredge sites, five fracture zones, and two drill sites and is strongly skewed toward slow spreading ridges. The modal abundance of olivine varies from 65 to 84 vol%, while orthopyroxene and clinopyroxene range from 26 to 14, and 11 to <1 vol%, respectively. Although these modal variations, on scales of 10–100 km^2, are almost universally thought to reflect varying degrees of adiabatic melting [1], a potential danger of averaging multiple thin section modes from a given site is that we may be masking real small-scale petrologic variations. However, as discussed below, the use of individual thin section modes leads to very similar trends in major-element bulk compositions.

2.2. *Compositions of olivine, pyroxene, and spinel in abyssal peridotites*

Abyssal peridotites are often so thoroughly serpentinized that primary crystals for some of the phases are completely obliterated. In fact, only 11 of the 43 modes in our data set are accompanied by a complete set of analyses, and less than half of the 75 thin section modes reported by Dick [7] have an associated olivine analysis. Thus, the calculation of a primary bulk composition for most of the modes in our data set requires the calculation of mineral compositions for one or more of the primary phases. Our method, following that of Dick and co-workers [1], is based on correlations between mineral compositions and olivine modes. Where no significant correlation is observed (e.g., Mn in all four phases and Ti in spinel), we averaged the entire population of individual analyses regardless of whether or not modal data were available. Since our objective is to determine the primary bulk compositions of abyssal peridotites, closed system exchange between primary phases during cooling has no effect on our determinations provided that all samples at a given olivine fraction equilibrated at similar temperatures. Based on limited two-pyroxene geothermometry, this appears to be the case [20].

Our calculation of olivine compositions begins with the positive correlation between site-averaged $(Mg\#)^{oliv}$ [(Mg/(Mg + Fe^*) in olivine] and modal olivine (Fig. 1), which is a natural consequence of the progressive melting of peridotite [21]. Note that the errors on the modal olivine contents in Fig. 1 are substantially larger than those associated with $(Mg\#)^{oliv}$, reflecting the large variations in modes seen in multiple thin sections from a given site. This indicates that a small number of thin sections are much less successful at capturing the average mode of a site than a small number of olivine analyses are at capturing the mean olivine composition. We used the modal olivine content at a given site, and the correlation in Fig. 1 to obtain $(Mg\#)^{oliv}$. Concentrations of Mn, Ca, and Ni were taken as the average for all individual analyses in our data set because a nonparametric statistical test [22] indicates a lack of correlation with modal olivine. The lack of an otherwise expected Ni–modal olivine correlation appears to reflect analytical difficulties and inconsistencies among the data sources. Silicon was fixed at 33.333% of the cations by assuming an ideal stoichiometry of $(Mg,Fe,Mn,Ca,Ni)_2SiO_4$ and Mg and Fe were computed from $(Mg\#)^{oliv}(66.667 - Mn - Ca - Ni)$ and $(1-(Mg\#)^{oliv})(66.667-Mn-Ca-Ni)$, respectively. Results for all elements are given in Table 1. Specific

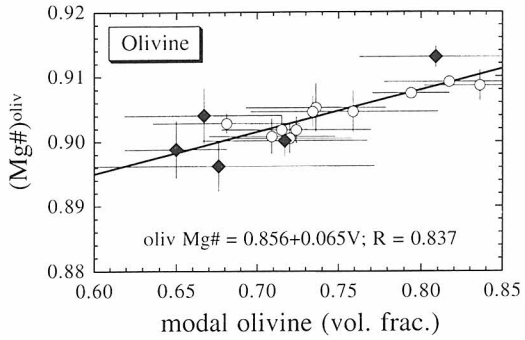

Fig. 1. $(Mg\#)^{oliv}$ versus modal olivine (as volume fraction) in abyssal peridotites. Open circles represent data from Dick and co-workers [1,5,16] and filled diamonds those of Bonatti and co-workers [2,19,40]. The solid line and equation refer to an unweighted least-squares fit to all of the data points with a Pearson correlation coefficient R. We used an unweighted regression in this and in succeeding figures because the errors on individual points are often poorly constrained. Data of Bonatti and co-workers represent fracture zone or drill hole averages [2,19,40], each of which is characterized by eight or more petrographic thin sections. Modal olivine values of [1,5,16] are averages from at least three large (24 cm^2) thin sections representing a dredge site or drill hole. For two dredge sites from the Atlantis II Fracture Zone, modal data from an adjacent dredge site were included in the average (RC27-9-6 + RC27-9-18 and RC27-9-44 + RC27-9-46) to satisfy the minimum sample requirement. Points lacking error bars on the olivine composition are based on analyses from one thin section. Also, unless otherwise noted, error bars in this and succeeding figures represent 1σ on the distributions.

procedures for the other three primary phases are described in the **EPSL Online Background Dataset** [1], hereafter referred to as the Appendix, and results for each element in each phase are given in Table 1.

2.3. Bulk compositions of abyssal peridotites

We calculated primary bulk compositions for each of 43 site-averaged modes after first computing phase compositions of minerals for which analyses were not available, converting these from cation to weight percents, and transforming the phase proportions from volume to weight fractions. The mineral density algorithms required for the latter operation are given in the Appendix. Since a large fraction of the calculated bulk compositions include contributions from one or more calculated mineral compositions, we first assess whether or not our mineral calculation scheme introduces a systematic bias and then compare our results to those of previous workers.

We calculated primary bulk compositions for each of eleven modes for which analyses of all phases are available using both mineral compositions as analyzed and calculated values for all four phases. Bulk values of Al_2O_3 are shown in Fig. 2a. The location of a particular point reflects how the calculated $(Al)^{opx}$ and, to a much lesser extent, $(Al)^{cpx}$ and $(Al)^{sp}$ compare to the averaged analyses for each phase from that site. Although not shown, CaO, TiO_2, Cr_2O_3, and Na_2O plots are similar in appearance to Fig. 2a in that points are distributed both above and below the 1 : 1 line. TiO_2, Cr_2O_3, and Na_2O display considerably more scatter than either Al_2O_3 or CaO, however, due to greater deviations between the site-averaged concentrations and their respective modal olivine regression lines. For SiO_2 (Fig. 2b), bulk compositions of samples obtained using the analyzed minerals are generally slightly lower than those for the calculated mineral compositions. This mostly reflects the fact that the analyzed olivine compositions are slightly low in silica relative to stoichiometric olivine (i.e., cation% of SiO_2 < 33.33%) so that SiO_2 calculated assuming the formula $(Mg,Fe,Mn,Ca,Ni)_2SiO_4$ is high by 0.1–0.2 wt%. Although not shown, MgO abundances generally plot a little below the 1 : 1 line. These negative deviations are consistent with the positive deviations observed for SiO_2, and also arise from a slight non-stoichiometry in the analyzed olivines.

For FeO^* (Fig. 2c), deviations from the 1 : 1 line reflect a sensitivity of calculated bulk FeO^* to small differences between the analyzed Mg#s for olivine and orthopyroxene versus those calculated using the modal-olivine based regressions. The deviations appear so dramatic for FeO^* because $(Mg\#)^{oliv}$ and $(Mg\#)^{opx}$ in abyssal peridotites are relatively high. If, for example, $(Mg\#)^{oliv}$ increases from 0.898 to 0.908 (cf. Fig. 1), $(MgO)^{oliv}$ increases by only 1.5% relative but $(FeO^*)^{oliv}$ decreases by 10%. This effect can be seen more clearly in Fig. 3, which shows that the percent deviation in $(FeO^*)^{bulk}$ is strongly correlated with the weighted sum of $\Delta(Mg\#)^{oliv}$ and

[1] http://www.elsevier.nl/locate/epsl, mirror site: http://www.elsevier.com/locate/epsl

Table 1
Mineral cation values and equations used to calculate abyssal peridotite bulk compositions

Mineral	Ti	Al	Cr	Fe^{3+}	Mn	Ca	Na	Ni
Oliv [a]	nr	nr	nr	nc	0.10 (3)	0.04 (4)	nr	0.24 (3)
Opx [b]	eqn [b]	eqn [b]	0.52 (12)	nc	0.09 (2)	2.03 (30)	eqn [b]	0.06 (2)
Cpx [c]	eqn [c]	eqn [c]	0.86 (16)	nc	0.07 (2)	18.9 (9)	eqn [c]	0.04 (2)
Sp [d]	0.06 (8)	eqn [d]	eqn [d]	eqn [d]	0.12 (6)	nr	nr	0.17 (10)

Abbreviations: nr = not regressed; nc = not calculated; eqn indicates that the cation value is defined as a function of modal olivine (expressed as volume fraction) using one of the equations listed below. All equations were calculated using mineral compositions averaged for each dredge site, fracture zone, and drill core. Equations are used to calculate cation values that showed a statistically significant correlation with modal olivine (as defined by a Spearman rank correlation at a 95% confidence level). Listed values are the calculated means for those cations that are not correlated with modal olivine; the numbers in parentheses are one standard deviation in terms of the least units cited, e.g., 0.10 (3) = 0.10 ± 0.03. Individual analyses were used to calculate mean values. Analyses of olivine, pyroxene, and spinel are from [2,4,5,7,10,11,13,15,16,37,38]. In a number of studies [4,5,11,13,15,16,37], selected minor elements were not analyzed in certain phases. The mean Ni content in olivine is based on analyses from [5,10,13,37,39]. The mean Ca values for orthopyroxene and clinopyroxene are based on analyses of fused minerals from Dick [7].

[a] Oliv: Mn and Ca based on 88 analyses and Ni on 35 analyses.

[b] Opx: $Ti = \exp(3.424 - 9.430V)$, where V represents the volume fraction of modal olivine; $Al = 16.060 - 15.741V$, which excludes RC27-9-44&46; Cr and Mn based on 165 analyses each; Ca based on 56 analyses of fused grains; Ni based on 122 analyses; $Na = 0.270 - 0.313V$, which excludes IO11/76-59 and IO11/76-60.

[c] Cpx: $Ti = \exp(2.155 - 8.354V^2)$, which excludes DSDP 556; $Al = 19.730 - 18.907V$; Cr and Mn based on 165 analyses each; Ca based on 43 analyses of fused grains; $Na = 5.276 - 6.199V$; Ni based on 89 analyses.

[d] Sp: Cr and Al are calculated using Cr# and spinel stoichiometry, see Fig. 3a and discussion in text; $Fe^{3+} = -4.973 + 9.693V$; Ti, Mn, and Ni based on 175, 134, and 171 analyses, respectively.

$\Delta(Mg\#)^{opx}$. The Delta values are the differences between the average of the measured Mg#s at a given site and those calculated using the Mg#–modal olivine regression lines. Thus, observed deviations from the 1:1 line in Fig. 2c simply reflect the differing extents to which the average olivine and orthopyroxene compositions deviate from Mg#s predicted by the modal olivine regressions, and the fact that small changes in Mg# produce relatively large changes in $(FeO^*)^{oliv}$ and $(FeO^*)^{opx}$. In spite of the systematic deviations apparent in Fig. 2c, the relative errors in $(FeO^*)^{bulk}$ are quite small (0.4–3.4%) and we show below that this introduces no significant artifacts into trends described from the calculated bulk compositions. We conclude that the relative errors introduced by our mineral calculation scheme are small for the major elements (mean values are 0.5% SiO_2, 0.5% MgO, 1.5% FeO^*, 4.7% CaO, 9.0% Al_2O_3, 12% Cr_2O_3, 31% TiO_2, 41% Na_2O).

Fig. 4 shows our calculated bulk compositions for major and minor oxides in abyssal peridotites plotted against bulk MgO (all in wt%). The first feature to note is that bulk compositions obtained using calculated mineral compositions (open or shaded circles) are consistent with those in which all phases were analyzed (closed circles). This is an important statement of internal consistency for our calculation scheme (i.e., systematic errors shown in Fig. 2 do not translate into significant systematic errors in Fig. 4). It is also notable that the impact of correcting for volume changes resulting from isochemical alteration on oxide-MgO plots appears to be modest. This is illustrated in Fig. 4 by line segments joining corrected (filled triangle) and uncorrected (filled circle) modes for ODP 895 data of [16]. Olivine is more thoroughly altered at this site than orthopyroxene (74% versus 64%) and the corrected mode contains 2.5% less modal olivine (on an absolute basis) leading to (1) lower bulk MgO, FeO^*, and NiO, (2) higher SiO_2, Al_2O_3, Cr_2O_3, and CaO; and (3) essentially unchanged TiO_2 and Na_2O. For SiO_2–, Al_2O_3–, CaO–, and NiO–MgO, the line segment between corrected and uncorrected modes is either coincident with or sub-parallel to the trend defined by all of the uncorrected modal compositions. Although not shown in Fig. 4, we also calculated bulk compositions for individual thin section modes after refitting the phase composition versus modal olivine expressions using data from individual thin sections [4,5,7,16]. With the exception of FeO^*–MgO, the

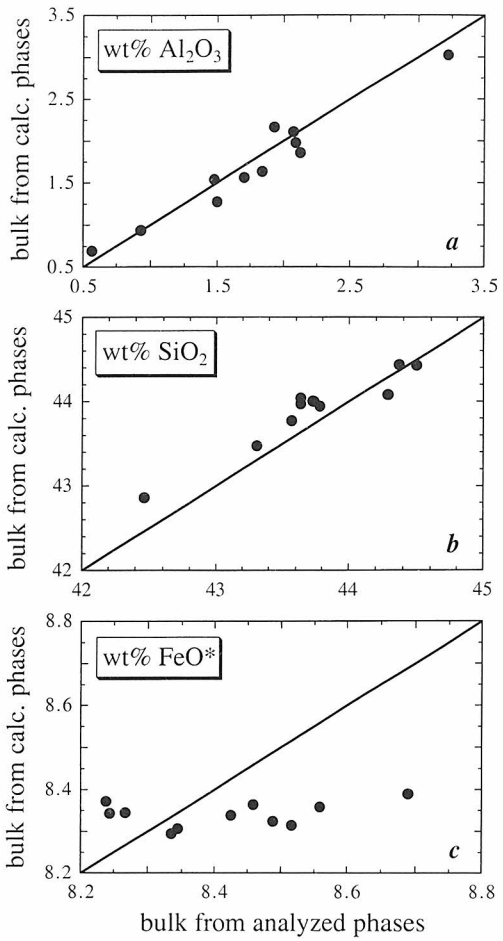

Fig. 2. A comparison of bulk compositions for abyssal peridotites calculated using averages of reported mineral compositions for olivine, clinopyroxene, orthopyroxene, and spinel [2,5,7,16] with those obtained using calculated phase compositions. A diagonal 1 : 1 line is shown in each panel. (a) Al_2O_3. (b) SiO_2. (c) FeO^*.

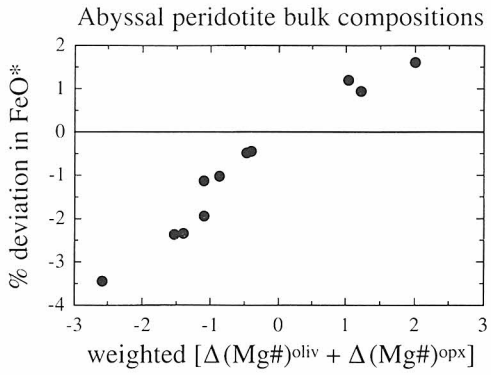

Fig. 3. Percent deviation in $(FeO^*)^{bulk}$ between calculated and analyzed phase compositions (Fig. 2c) versus the weighted sum of $\Delta(Mg\#)^{oliv} + \Delta(Mg\#)^{opx}$, given by the expression: $1000[(\text{modal oliv})(\text{anal}(Mg\#)^{oliv} - \text{reg}(Mg\#)^{oliv}) + (\text{modal orthopyroxene})0.63(\text{anal}(Mg\#)^{opx} - \text{reg}(Mg\#)^{opx})]$, where 'anal' and 'reg' refer to Mg#s calculated from actual analyses and modal olivine regression equations, respectively, and modal values are in weight fractions. The 0.63 represents the ratio of the average $(FeO^*)^{opx}$ to the average $(FeO^*)^{oliv}$ in our suite of abyssal peridotites.

two data sets completely overlap. Even for FeO^*–MgO, there is considerable overlap although the trend for individual samples displays a slight positive slope (FeO^* varies from 8.1 to 8.5% between 40.5 and 48.5% MgO; see Appendix). We conclude that using site averages rather than individual thin sections does not introduce a major bias.

Our calculated values for bulk SiO_2, Al_2O_3, TiO_2, and Na_2O in abyssal peridotites all decrease with increasing MgO (Fig. 4), while Cr_2O_3–MgO and FeO^*–MgO trends are essentially horizontal. Although not shown in Fig. 4, bulk CaO is negatively correlated with MgO while the bulk NiO–MgO trend defines a positive correlation (both of these trends are also linear). All of these relationships are qualitatively consistent with those expected for high-pressure partial melting of peridotites [25,26]. The curved Na_2O–MgO and TiO_2–MgO trends are qualitatively consistent with fractional melting [14]. The essentially linear trends (SiO_2–, Al_2O_3–, Cr_2O_3–, FeO^*–, CaO–, and NiO–MgO) are consistent within error of estimated compositions for primitive upper mantle, and either overlap or closely parallel regression lines based on a global ultramafic nodule and peridotite massif data set. Since the major-element variations in the global suite are widely interpreted as reflecting the extraction of basaltic melt [23], most of the trends shown by abyssal peridotites can, to first order, be interpreted in the same way (the linear and elevated TiO_2– and Na_2O–MgO trends of the global suite suggest processes in addition to partial melting).

For the most part, there is good agreement between our results and those of Niu et al. [8]. The slope of our SiO_2–MgO trend is slightly shallower than theirs [8], and our calculated bulk compositions tend to hug the high-silica side of their data. This reflects slightly higher Mg#s (and thus, higher SiO_2

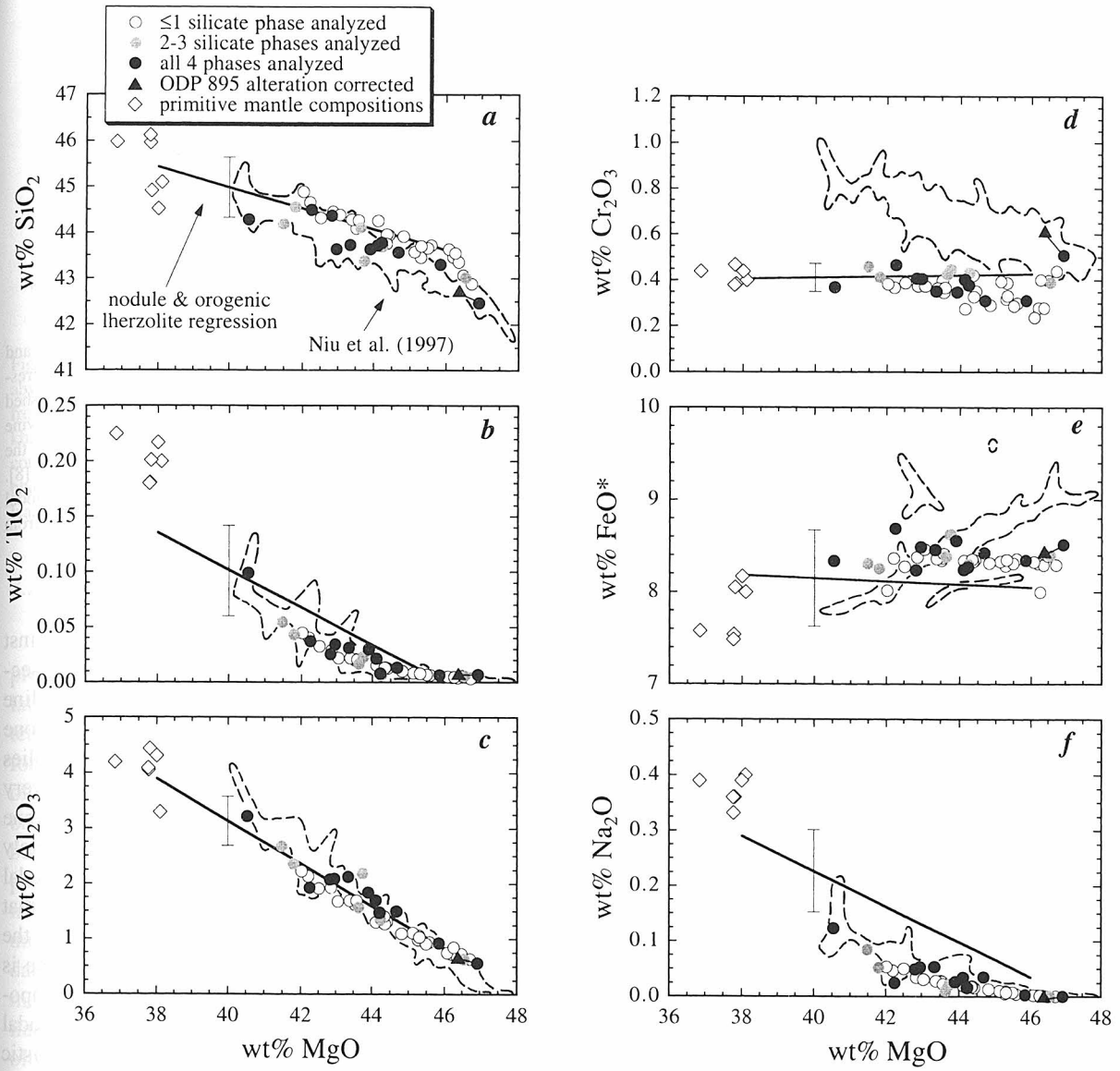

Fig. 4. Primary bulk compositions of site-averaged abyssal peridotites as a function of MgO. Filled circles represent bulk compositions calculated from the modal data and averages of reported mineral compositions for olivine, orthopyroxene, clinopyroxene, and spinel. Open circles denote bulk compositions calculated using reported averages for one and shaded circles for two or three of the primary silicate phases with the remaining phase compositions being calculated as described in the text and Appendix. Dashed lines enclose calculated abyssal peridotite compositions from Niu et al. [8]. Only those samples whose bulk compositions were predicted from reported clinopyroxene compositions were used to define the Niu et al. [8] fields. The filled triangle denotes the bulk composition of site ODP 895 calculated using mineral modes corrected for alteration by [16]. A thin solid line connects the corrected and uncorrected bulk compositions. Open diamonds represent estimates of the bulk composition of primitive mantle [41–46]. Thick solid lines are unweighted linear fits obtained by minimizing the sum of the absolute deviations to a global suite of 460 spinel lherzolite and harzburgite analyses from ultramafic nodules and peridotite massifs [47]. Error brackets denote the mean deviation between an oxide in this data set and the regression line. (a) SiO_2. (b) TiO_2. (c) Al_2O_3. (d) Cr_2O_3. (e) FeO^*. (f) Na_2O.

contents) in our calculated silicates and perhaps the differences in our approaches for calculating mineral compositions. However, for Cr_2O_3 and FeO^*, our results differ substantially from those of Niu et al. [8]. We have no explanation for the anomalously high Cr_2O_3 of [8] but note that their results are difficult to reconcile with estimated Cr_2O_3 in primitive mantle without invoking processes other than simple partial melting. The differences for FeO^*–MgO variations (Fig. 4e) are both startling and important. Our compositions form a nearly horizontal array as do bulk compositions of abyssal peridotites calculated by Elthon [14]. In contrast, the data of Niu et al. [8] define an array with a strikingly positive slope, which led them to postulate the addition of olivine on a hand-sample scale via crystallization during porous flow of melt through the peridotite matrix. The FeO^*–MgO trend defined by our calculated abyssal peridotite compositions is inconsistent with such an interpretation.

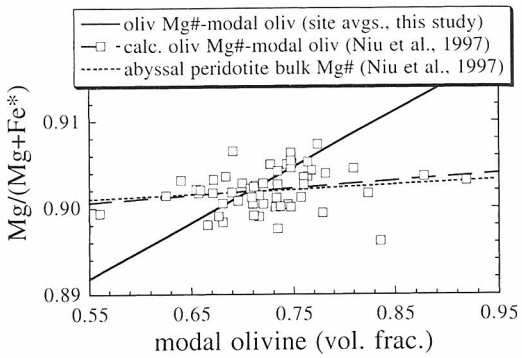

Fig. 5. Correlation between Mg# (either olivine or bulk rock) and modal olivine content. The solid line is the site-averaged regression from Fig. 1. Open squares and accompanying long-dashed regression line show the relationship between modal olivine in individual thin sections and $(Mg\#)^{oliv}$ calculated using the $(Mg\#)^{oliv}$–$(FeO^*)^{opx}$ equation in the appendix of Niu et al. [8]. The short-dashed line is a regression of $(Mg\#)^{bulk}$ versus modal olivine using the calculated abyssal peridotite compositions from [8].

3. Discussion

3.1. $(Mg\#)^{oliv}$ versus modal olivine in abyssal peridotites

The crux of the analysis presented by Niu and co-workers concerning the origin and evolution of abyssal peridotites [8,24] rests on the validity of their bulk FeO^*–MgO relationship. Since our results appear to be inconsistent with theirs for this critical oxide pair, it is important that we first explore why the trends in Fig. 4e are so different before considering further implications of our own results for processes in the Earth's upper mantle. Niu et al. [8] generated expressions relating clinopyroxene compositions to those of other primary phases because clinopyroxene is the most commonly analyzed relict silicate in abyssal peridotites. Since the calculated $(Mg\#)^{bulk}$ of a peridotite (perid) is essentially that of olivine (i.e., $(Mg\#)^{perid}/(Mg\#)^{oliv} \approx 1$), the key features of their bulk Mg#s (and hence FeO^* contents) are a direct consequence of their calculated values for $(Mg\#)^{oliv}$. Niu et al. [8] have not published their expression relating $(Mg\#)^{oliv}$ to the composition of clinopyroxene, but they do provide an equation relating $(Mg\#)^{oliv}$ to orthopyroxene compositions. Fig. 5 shows the resulting $(Mg\#)^{oliv}$s plotted against the modal olivine contents of individual thin sections. The fact that the corresponding regression line (long dashes) is nearly indistinguishable from one based on the bulk Mg#s of Niu et al. [8] implies that the $(Mg\#)^{oliv}$–orthopyroxene relationship is very similar to the unreported $(Mg\#)^{oliv}$–clinopyroxene regression. Neither line (Fig. 5) comes remotely close to describing the real variation between modal olivine and $(Mg\#)^{oliv}$. The essential problem is that while $(FeO^*)^{opx}$ and $(Mg\#)^{oliv}$ are correlated, the correlation between $(FeO^*)^{opx}$ and modal olivine is very weak. This leads to calculated olivine compositions that are virtually independent of the modal olivine content (Fig. 5), a feature not characteristic of abyssal peridotites (Fig. 1). A virtually constant olivine composition also creates what amounts to a mixing line between an olivine with ~9.5 wt% FeO and ~49 wt% MgO and a mixture of orthopyroxene, clinopyroxene, and spinel with ~6 wt% FeO and ~31 wt% MgO. Varying the percentage of olivine along this mixing line reproduces the positive slope exhibited by the data of Niu et al. [8] in Fig. 4e. We conclude that the distribution of FeO^*–MgO values obtained by Niu et al. [8] is an artifact of their calculation scheme and that it should not be used as a basis for understanding processes in the upper mantle.

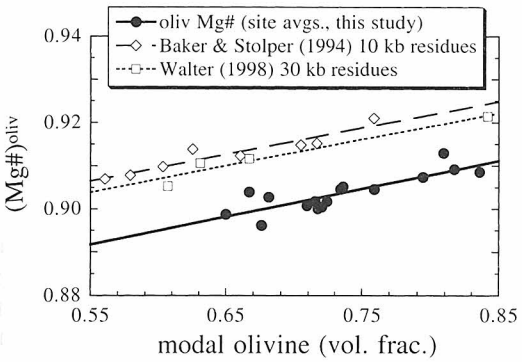

Fig. 6. $(Mg\#)^{oliv}$ versus modal olivine (volume fraction) in abyssal peridotites (same points as in Fig. 1) and in the residues from isobaric peridotite melting experiments at 10 [25] and 30 kbar [26]. Residual phase proportions in the experiments were converted from weight units to volume units using calculated phase densities (see Appendix). The three lines are unweighted least-squares fits to their associated data sets.

3.2. Partial melting signatures in abyssal peridotites

High-pressure melting experiments on peridotites provide a qualitative assessment of the functional relationship between $(Mg\#)^{oliv}$ and modal olivine content. Fig. 6 compares $(Mg\#)^{oliv}$–modal olivine trends for our site-averaged abyssal peridotites with those of experimental residues produced during isobaric batch melting at 10 and 30 kbar [25,26]. Although both experimental trends are off-set from the abyssal peridotite regression line (reflecting differences in initial $(Mg\#)^{bulk}$ and possibly alteration-induced volume expansion in the abyssal peridotites), all three data sets have similar slopes. Given the differences in melt compositions and melting processes, these similarities in slope suggest that the $(Mg\#)^{oliv}$–modal olivine trend is not very sensitive to the depth of melting or the melting process. Nevertheless, the observed correlation for abyssal peridotites most likely reflects partial melting and not a refertilization process. If large volumes of fresh basaltic melt moved through each rock [14], the olivine would tend to equilibrate to a constant Mg# independent of the volume fraction of olivine. Such a process would produce a nearly horizontal line in Fig. 1 contrary to the observed trend. It is also important to note that TiO_2 and Na_2O define curved trends in Fig. 4, and plot below the global regression lines. Extensive refertilization would be expected to produce linear trends for these oxides through what is essentially a mixing process involving basaltic melt and previously depleted peridotite. Thus, our data do not support the suggestion of Elthon [14] that abyssal peridotites have experienced pervasive refertilization.

3.3. Metasomatic signals in abyssal peridotites

There is abundant geochemical evidence that many samples in peridotite massifs and the mantle sections of ophiolites interacted with melts during or after partial melting [27,28]. While the presence of plagioclase and fertile mineral compositions in plagioclase-bearing abyssal peridotites indicates a component of trapped melt [7,19], the case for plagioclase-free abyssal peridotites is more subtle. Site-averaged concentrations of $(Na_2O)^{bulk}$ in plagioclase-free abyssal peridotites decrease with increasing modal olivine content (Fig. 4f), but sodium is still enriched relative to residual compositions calculated assuming simple models of polybaric near-fractional melting [8,14,24]. Moreover, while variations in mineral Mg#s are relatively restricted at any given locality (Fig. 1), $(Ti)^{cpx}$ can vary by nearly a factor of three and $(Na)^{cpx}$ by more than an order of magnitude (Fig. 7). Since $(Ti)^{cpx}$ in abyssal peridotites is generally also positively correlated with $(Na)^{cpx}$ at a given site (in contrast to Na versus Al or Mg#), it seems likely that the wide range in Na–Ti concentrations at each locality reflects metasomatic processes, what Kelemen et al. [6] refer to as diffuse reactive porous flow. These processes appear to be localized since $(Na)^{cpx}$ and $(Ti)^{cpx}$ from the same dredge haul, and sometimes even from the same thin section, can vary greatly. The implication for abyssal peridotites is that the minimum $(Na)^{cpx}$ and $(Ti)^{cpx}$ at any given olivine content is more likely to reflect adiabatic partial melting than the average value.

To test the extent to which variable Na–Ti signatures in pyroxene influence bulk values, we calculated new peridotite bulk compositions using equations describing a lower-bound fit for $(Na)^{cpx}$ and a corresponding curve for $(Ti)^{cpx}$ (Fig. 7). Since the lower bounds are poorly constrained, the solid curves in Fig. 7 are most likely loose upper bounds on the true minima. Given the wide range of sodium values at any particular modal olivine content, we, also obtained an 'extreme' lower bound for $(Na)^{cpx}$ based

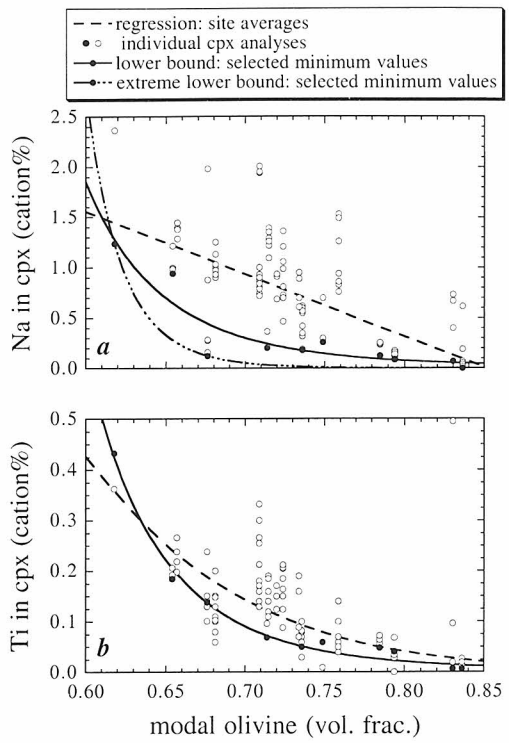

Fig. 7. (a) Sodium and (b) titanium values (cation %) from individual clinopyroxenes for each of the dredge sites, fracture zones, and drill holes versus the average modal olivine content at each site. Dashed curves are unweighted least-squares regressions (see Appendix) based on the average clinopyroxene composition at each site. The solid curve in (a) is an unweighted least-squares fit to the filled circles, representing minimum $(Na)^{cpx}$ from the following sites: RC27-9-30, RC27-9-34, RC27-9-35 (Atlantis II FZ); Vulc 5-34, Vulc 5-35 (NE Bullard FZ); AII107-40 (Bouvet FZ); Owen FZ; W. Romanche FZ; DSDP 556; ODP 895. $(Na)^{cpx} = \exp(-12.084 + 7.621/V)$, where V represents modal olivine in volume fraction. The dot–dashed line in (a) is an unweighted least-squares fit to the W. Romanche FZ, Owen FZ, and ODP 895 data defining an 'extreme' lower bound with an equation $(Na)^{cpx} = \exp(-26.608 + 16.575/V)$. In (b), the lower bound (solid) curve $[(Ti)^{cpx} = \exp(-14.109 + 8.135/V)]$ was computed using the same analyses as were used to define the lower bound for sodium.

on three sites. Note that the lower bound for $(Ti)^{cpx}$ (Fig. 7b) was defined using the same clinopyroxene analyses that defined the $(Na)^{cpx}$ minima. While Ti and Na are broadly correlated in abyssal peridotite clinopyroxenes, grains with minimum sodium values at each site do not necessarily have the lowest titanium contents. Nevertheless, the solid curve in Fig. 7b is, on average, within 20% of the least-squares fit that would result if the minimum Ti value was used at each site. Because minimum sodium and titanium contents in orthopyroxene are zero (i.e., below detection limits) in our data set at modal olivine contents greater than 0.7, we calculated average $(Na)^{opx}/(Na)^{cpx}$ and $(Ti)^{opx}/(Ti)^{cpx}$ ratios using the least-squares fits to the average orthopyroxene and clinopyroxene compositions (Table 1) and modal olivine contents between 0.62 and 0.84, incremented in units of 0.02. Our calculated values for $(Na)^{opx}/(Na)^{cpx}$ and $(Ti)^{opx}/(Ti)^{cpx}$ (0.060 ± 0.013 and 0.33 ± 0.07, respectively) overlap with those calculated using analyses of equilibrated orthopyroxenes and clinopyroxenes from mantle nodules [29–32].

Fig. 8 compares modified bulk Na_2O and TiO_2 compositions to the original values and those of plagioclase-bearing and plagioclase-free spinel lherzolites from the Eastern Romanche Fracture Zone [19] that are widely thought to have experienced basaltic melt refertilization [7,19]. At ~41 wt% MgO, Na_2O in the four sets of peridotite compositions spans approximately an order of magnitude, while at 46 wt% MgO, Na_2O contents differ by as much as three orders of magnitude. Variations are less extreme for TiO_2, but still up to an order of magnitude at constant MgO. Fig. 8 also shows calculated residual mantle compositions using the models of [33,34]. These simple end-member melting models assume constant melt productivity and no re-equilibration between melts and residues. Bulk Na–Ti for the Romanche Fracture Zone are substantially higher than those for calculated residues, consistent with extensive refertilization of these rocks and the conclusions of [7,19]. For 'normal' abyssal peridotites, both site-averaged TiO_2 values and those based on the lower bound in Fig. 7b are consistent within error of the calculated residues (i.e., evidence for a metasomatic signature rests primarily on variability and correlations with sodium). As noted by others [8,14,24], calculated sodium residues are inconsistent with bulk Na_2O contents calculated using site-averaged pyroxene compositions. However, concentrations calculated using lower and 'extreme' lower bounds on $(Na)^{cpx}$ bracket the model residues. Thus, Na–Ti contents of clinopyroxenes in abyssal peridotites may contain information on both initial partial melting and on diffuse reactive porous flow.

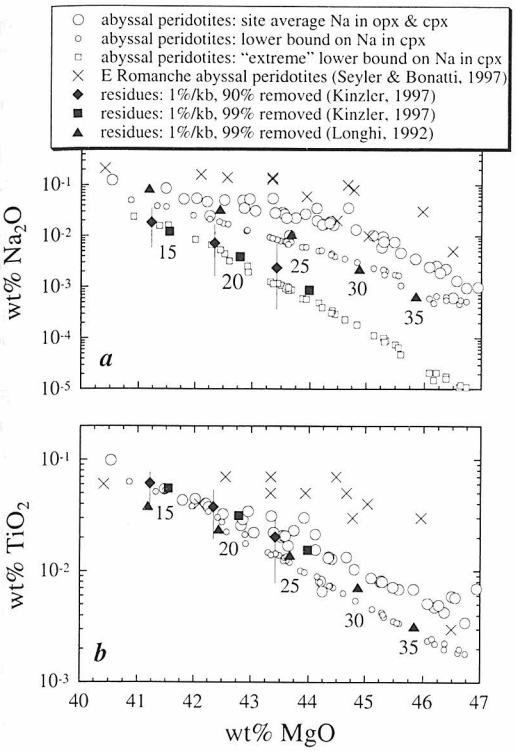

Fig. 8. Variation diagram showing bulk (a) Na_2O and (b) TiO_2 in abyssal peridotites and in residual mantle compositions as a function of bulk MgO content (wt%). Large open circles refer to the same abyssal peridotites plotted in Fig. 4. Small open circles and squares denote lower and 'extreme' lower bounds for abyssal peridotites (equations in the caption to Fig. 7). Concentrations in orthopyroxene were calculated using average concentration ratios for opx/cpx as discussed in the text. Residual mantle compositions were calculated using the melting models of Kinzler [33] and Longhi [34], the latter incorporating high-pressure experimental data of Longhi [48]. For [33], we modified the expressions for sodium and titanium partition coefficients between pyroxene/liquid (see Appendix for equations and data sources). For all calculations, the starting composition was a primitive mantle with 0.36 wt% Na_2O and 0.15 wt% TiO_2. Both values are within the range of primitive mantle estimates [49]. The number by each diamond denotes P_o, the pressure (in kbar) at which the ascending mantle crosses the solidus and marks the point at which melting begins. No 30 or 35 kbar calculations were done using the Kinzler model since it does not include garnet. For both models, the mantle was assumed to melt 1%/kbar and either 90% or 99% of the melt was removed at each step and melting was stopped when the pressure reached 3 kbar. Thus, each plotted point represents the composition of residual mantle at 3 kbar, i.e., at the top of the melting column. The choice of 3 kbar is arbitrary but consistent with thermal modeling beneath mid-ocean ridges [50]. Error bars associated with filled diamonds show the effect of varying the pyroxene Na and Ti partition coefficients by ±35%. The differences in the calculated sodium residues between the two models reflect differences and in $D_{Na}^{opx/liq}$ residual modal mineralogy.

We hesitate to place too much emphasis on a comparison between calculated residues and our calculated bulk compositions because the appropriate sodium contents are uncertain and it is difficult to predict how uncertainties in the melting models affect the residual bulk compositions. Also, recent work [35,36] suggests that melting and transport processes may be much more complex than generally assumed in current models of polybaric melting of peridotites. It nevertheless seems likely that the Na_2O abundances in abyssal peridotites calculated using the mean pyroxene compositions are higher than those predicted by any melting model that does not postulate melt-residue re-equilibration. The widely varying Na_2O contents in abyssal peridotites appear to support the conclusions of Kelemen et al. [6] that mantle partial melts move via at least two transport mechanisms beneath mid-ocean ridges.

Acknowledgements

This work was supported by NSF grant OCE-9529878 and NASA grant NAG5-4318. Discussions with K. Nolan and formal reviews by D. Francis, F. Frey, and K. Johnson are gratefully acknowledged. *[FA]*

References

[1] H.J.B. Dick, R.L. Fisher, W.B. Bryan, Mineralogic variability of the uppermost mantle along mid-ocean ridges, Earth Planet. Sci. Lett. 69 (1984) 88–106.

[2] P.R. Hamlyn, E. Bonatti, Petrology of mantle-derived ultramafics from the Owen Fracture Zone, Northwest Indian Ocean: implications for the nature of the oceanic upper mantle, Earth Planet. Sci. Lett. 48 (1980) 65–79.

[3] H.J.B. Dick, R.L. Fisher, Mineralogic studies of the residues of mantle melting: abyssal and alpine-type peridotites, in: J. Kornprobst (Ed.), Kimberlites II: The Mantle and Crust–Mantle Relationships, Elsevier, Amsterdam, 1984, pp. 295–308.

[4] K.T.M. Johnson, H.J.B. Dick, N. Shimizu, Melting in the oceanic upper mantle: an ion microprobe study of diopsides in abyssal peridotites, J. Geophys. Res. 95 (1990) 2661–2678.

[5] K.T.M. Johnson, H.J.B. Dick, Open system melting and temporal and spatial variation of peridotite and basalt at the Atlantis II Fracture Zone, J. Geophys. Res. 97 (1992) 9219–9241.

[6] P.B. Kelemen, G. Hirth, N. Shimizu, M. Spiegelman, H.J.B. Dick, A review of melt migration processes in the adiabatically upwelling mantle beneath oceanic spreading ridges, Philos. Trans. R. Soc. London, Ser. A 355 (1997) 283–318.
[7] H.J.B. Dick, Abyssal peridotites, very slow spreading ridges and ocean ridge magmatism, in: A.D. Saunders, M.J. Norry (Eds.), Magmatism in the Ocean Basins, Geol. Soc. Spec. Publ. 42 (1989) 71–105.
[8] Y. Niu, C.H. Langmuir, R.J. Kinzler, The origin of abyssal peridotites: a new perspective, Earth Planet. Sci. Lett. 152 (1997) 251–265.
[9] J.M. Sinton, Petrology of (alpine-type) peridotites from site 395, DSDP Leg 45, Init. Rep. DSDP 45 (1979) 595–601.
[10] T. Juteau, E. Berger, M. Cannat, Serpentinized, residual mantle peridotites from the M.A.R. median valley, ODP Hole 670A (21°10′N, 45°02′W, Leg 109): primary mineralogy and geothermometry, Proc. ODP, Sci. Results 106–109 (1990) 27–45.
[11] J.E. Snow, H.J.B. Dick, Pervasive magnesium loss by marine weathering of peridotite, Geochim. Cosmochim. Acta 59 (1995) 4219–4235.
[12] D.R. Janecky, W.E. Seyfried, Hydrothermal serpentinization of peridotite within the oceanic crust: experimental investigations of mineralogy and major element chemistry, Geochim. Cosmochim. Acta 50 (1986) 1357–1378.
[13] E. Bonatti, M. Seyler, N. Sushevskaya, A cold suboceanic mantle belt at the Earth's equator, Science 261 (1993) 315–320.
[14] D. Elthon, Chemical trends in abyssal peridotites: refertilization of depleted suboceanic mantle, J. Geophys. Res. 97 (1992) 9015–9025.
[15] P.J. Michael, E. Bonatti, Peridotite composition from the North Atlantic: regional and tectonic variations and implications for partial melting, Earth Planet. Sci. Lett. 73 (1985) 91–104.
[16] H.J.B. Dick, J.H. Natland, Late-stage melt evolution and transport in the shallow mantle beneath the East Pacific Rise, Proc. ODP, Sci. Results 147 (1996) 103–134.
[17] E.S. Larsen, F.S. Miller, The Rosiwal method and the modal determination of rocks, Am. Mineral. 20 (1935) 260–273.
[18] M.B. Bayly, Modal analysis by point-counter — the choice of sample area, J. Geol. Soc. Aust. 6 (1960) 119–129.
[19] M. Seyler, E. Bonatti, Regional-scale melt–rock interaction in lherzolitic mantle in the Romanche Fracture Zone (Atlantic Ocean), Earth Planet. Sci. Lett. 146 (1997) 273–287.
[20] L.T. Bryndzia, B.J. Wood, Oxygen thermobarometry of abyssal spinel peridotites: the redox state and C–O–H volatile composition of the Earth's sub-oceanic upper mantle, Am. J. Sci. 290 (1990) 1093–1116.
[21] E. Takahashi, T. Shimazaki, Y. Tsuzaki, H. Yoshida, Melting study of a peridotite KLB-1 to 6.5 GPa, and the origin of basaltic magmas, Philos. Trans. R. Soc. London, Ser. A 342 (1993) 105–120.
[22] W.H. Press, S.A. Teukolsky, W.T. Vetterling, B.P. Flannery, Numerical Recipes in FORTRAN, Cambridge University Press, Cambridge, 1992, 963 pp.
[23] W.F. McDonough, F.A. Frey, Rare earth elements in upper mantle rocks, in: B.R. Lipin, G.A. McKay (Eds.), Geochemistry and Mineralogy of Rare Earth Elements, Reviews in Mineralogy, 21, The Mineralogical Society of America, Washington, DC, 1989, pp. 99–145.
[24] Y. Niu, Mantle melting and melt extraction processes beneath ocean ridges: evidence from abyssal peridotites, J. Petrol. 38 (1997) 1047–1074.
[25] M.B. Baker, E.M. Stolper, Determining the composition of high-pressure mantle melts using diamond aggregates, Geochim. Cosmochim. Acta 58 (1994) 2811–2827.
[26] M.J. Walter, Melting of garnet peridotite and the origin of komatiite and depleted lithosphere, J. Petrol. 39 (1998) 29–60.
[27] J.-L. Bodinier, G. Vasseur, J. Vernieres, C. Dupuy, J. Fabries, Mechanisms of mantle metasomatism: geochemical evidence from the Lherz orogenic peridotite, J. Petrol. 31 (1990) 597–628.
[28] A.V. Sobolev, V.G. Batanova, Mantle lherzolites of the Troodos Ophiolite Complex, Cyprus: clinopyroxene geochemistry, Petrology 3 (1995) 440–448.
[29] T. Sachtleben, H.A. Seck, Chemical control of Al-solubility in orthopyroxene and its implications on pyroxene geothermometry, Contrib. Mineral. Petrol. 78 (1981) 157–165.
[30] J.-L. Bodinier, C. Dupuy, J. Dostal, C. Merlet, Distribution of trace transition elements in olivine and pyroxenes from ultramafic xenoliths: application of microprobe analysis, Am. Mineral. 72 (1987) 902–913.
[31] F.C. Bishop, J.V. Smith, J.B. Dawson, Na, K, P and Ti in garnet, pyroxene and olivine from peridotite and eclogite xenoliths from African kimberlites, Lithos 11 (1978) 155–173.
[32] K. Suzuki, Grain-boundary enrichment of incompatible elements in some mantle peridotites, Chem. Geol. 63 (1987) 319–334.
[33] R.J. Kinzler, Melting of mantle peridotite at pressures approaching the spinel to garnet transition: application to mid-ocean ridge basalt petrogenesis, J. Geophys. Res. 102 (1997) 853–874.
[34] J. Longhi, Origin of picritic green glass magmas by polybaric fractional fusion, Proc. Lunar Planet. Sci. 22rd, 1992, pp. 343–353.
[35] P.D. Asimow, M.M. Hirschmann, E.M. Stolper, An analysis of variations in isentropic melt productivity, Philos. Trans. R. Soc. London, Ser. A 355 (1997) 255–281.
[36] M. Spiegelman, Geochemical consequences of melt transport in 2-D: the sensitivity of trace elements to mantle dynamics, Earth Planet. Sci. Lett. 139 (1996) 115–132.
[37] E. Bonatti, A. Peyve, P. Kepezhinskas, N. Kurentsova, M. Seyler, S. Skolotnev, G. Udintsev, Upper mantle heterogeneity below the Mid-Atlantic Ridge, 0°–15°N, J. Geophys. Res. 97 (1992) 4461–4476.
[38] M. Cannat, D. Bideau, H. Bougault, Serpentinized peridotites and gabbros in the mid-Atlantic Ridge axial valley at 15°37′N and 16°52′N, Earth Planet. Sci. Lett. 109 (1992) 87–106.
[39] M. Cannat, D. Bideau, R. Hébert, Plastic deformation and

magmatic impregnation in serpentinized ultramafic rocks from the Garrett transform fault (East Pacific Rise), Earth Planet. Sci. Lett. 101 (1990) 216–232.

[40] E. Bonatti, P.J. Michael, Mantle peridotites from continental rifts to ocean basins to subduction zones, Earth Planet. Sci. Lett. 91 (1989) 297–311.

[41] A.E. Ringwood, Origin of the Earth and Moon, Springer, New York, 1979, 295 pp.

[42] S.-s. Sun, Chemical composition and origin of the earth's primitive mantle, Geochim. Cosmochim. Acta 46 (1982) 179–192.

[43] H. Wänke, G. Dreibus, E. Jagoutz, Mantle chemistry and accretion history of the earth, in: A. Kröner, G.N. Hanson, A.M. Goodwin (Eds.), Archaean Geochemistry: The Origin and Evolution of the Archaean Continental Crust, Springer, Berlin, 1984, pp. 1–24.

[44] S.R. Hart, A. Zindler, In search of a bulk-earth composition, Chem. Geol. 57 (1986) 247–267.

[45] C.J. Allègre, J.-P. Poirier, E. Humler, A.W. Hofmann, The chemical composition of the Earth, Earth Planet. Sci. Lett. 134 (1995) 515–526.

[46] W.F. McDonough, S.-s. Sun, The composition of the Earth, Chem. Geol. 120 (1995) 223–253.

[47] C.T. Herzberg, Lithosphere peridotites of the Kaapvaal craton, Earth Planet. Sci. Lett. 120 (1993) 13–29.

[48] J. Longhi, Liquidus equilibria of some primary lunar and terrestrial melts in the garnet field, Geochim. Cosmochim. Acta 59 (1995) 2375–2386.

[49] A. Zindler, S. Hart, Chemical geodynamics, Annu. Rev. Earth Planet. Sci. 14 (1986) 493–571.

[50] J. Phipps Morgan, E.M. Parmentier, J. Lin, Mechanisms for the origin of mid-ocean ridge axial topography: implications for the thermal and mechanical structure of accreting plate boundaries, J. Geophys. Res. 92 (1987) 12823–12836.